Supplementary Materials for

Structures of the nitrogenase complex prepared under catalytic turnover conditions

Hannah L. Rutledge, Brian D. Cook, Hoang P. M. Nguyen, Mark A. Herzik Jr*, F. Akif Tezcan[1]*

Correspondence to: tezcan@ucsd.edu (FAT), mherzik@ucsd.edu (MAH).

This PDF file includes:

Materials and Methods
Figs. S1 to S13
Tables S1 to S5

Materials and Methods

Protein expression and purification

Wild-type, untagged FeP and MoFeP were expressed in their native organism, *Azotobacter vinelandii* (*Av*) cells (strain DJ) using previously established protocols (*36*). Briefly, *Av* cultures were grown aerobically in Burk's media (181 mM sucrose, 0.9 mM $CaCl_2$, 1.7 mM $MgSO_4$, 35 μM $FeSO_4$, 2 μM $Na_2Mo_2O_4$, 0.2 mM citric acid, 10 mM K_3PO_4 pH 7.5, 3 mM NH_4Cl) in a 60 L fermenter at 30°C, 200 rpm. Cells were harvested and pelleted ~4 h after derepression of nitrogenase, as indicated by a spike in dissolved oxygen content. Cell pellets were stored at −80 °C until purification.

Cell lysis and protein purification were carried out under ultrahigh-purity Ar on a Schlenk line, or under a 95% Ar/5% H_2 mixture in a Coy Lab anaerobic chamber using previously established protocols (*1*). All buffers used were purged of air and stored under Ar. Cell pellets were resuspended in ~200 mL equilibration buffer (50 mM Tris pH 7.75, 200 mM NaCl, 5 mM sodium dithionite (NaDT), 0.1 mg/mL DNase I) prior to lysis with a microfluidizer at 16,000 psi Ar. The lysate was centrifuged at 12,000 rpm for 75 min. Both nitrogenase component proteins were purified from the supernatant by separation on a DEAE Sepharose column with a NaCl gradient (200 to 500 mM NaCl in 50 mM Tris pH 7.75, 5 mM NaDT). MoFeP eluted at ~25 mS/cm, and FeP eluted at ~30 mS/cm. Fractions containing nitrogenase proteins were brown in color and were verified by sodium dodecyl sulfate polyacrylamide gel electrophoresis (SDS-PAGE). Fractions containing FeP or MoFeP proteins were pooled and diluted two-fold with salt-free buffer (50 mM Tris, pH 7.75), then concentrated using a second, smaller DEAE Sepharose column by eluting with high salt buffer (500 mM NaCl, 50 mM Tris, pH 7.75, 5 mM NaDT). MoFeP and FeP were further purified with a Sepharose 200 gel filtration column (500 mM NaCl, 50 mM Tris, pH 8.0, 5 mM NaDT). Fractions containing pure protein were identified with SDS-PAGE. Purified protein was concentrated using an Amicon concentrator at 20 psi 95% Ar/5% H_2 using a 30 kDa and 100 kDa cutoff membrane for FeP and MoFeP, respectively. Purified proteins were syringe filtered through a 0.2 μm filter membrane. Protein concentrations were determined using Bradford assay and verified with an Fe chelation assay (6.2 M guanidine-HCl, 2 mM 2,2'-bipyridine, 10% glacial acetic acid) by measuring absorption at 522 nm and using an extinction coefficient of 8650 M^{-1} cm^{-1}, using 4 Fe per FeP and 30 Fe per MoFeP in stoichiometric calculations. Purified proteins were determined to be fully active through C_2H_2 reduction assays which were performed through gas chromotagraphy measurements as previously described (*36*); the specific activity of the stock MoFeP for C_2H_2 reduction was 1600 nmol C_2H_4 produced per minute per mg of MoFeP. Purified proteins were stored under liquid N_2 and underwent only one freeze-thaw cycle before use.

Turnover sample preparation for cryoEM analysis

FeP and MoFeP stock solutions were exchanged into reaction buffer (20 mM Tris, pH 8.0, 25 mM NaCl, anaerobic) and concentrated using 30 kDa and 100 kDa Microcon centrifugal filters, respectively, in a Coy anaerobic chamber (95% Ar, 5% H_2). Protein concentrations were measured using an Fe chelation assay. All reaction component stock solutions were made, syringe-filtered (0.2 μm filter), and degassed with ultra-high-purity N_2 immediately prior to use.

To prepare turnover samples, MoFeP was transferred from 95% Ar/ 5% H_2 atmosphere into sealed reaction vials under ultra-high-purity N_2 atmosphere using Hamilton gas-tight syringe after reaction components ($MgCl_2$, Na_2ATP, NaDT, and NaCl in Tris pH 8.0, and in some samples NaF and $BeSO_4$) had been mixed. Catalysis was initiated in the turnover and BeF_x-inhibited samples

by addition of FeP with Hamilton gas-tight syringe after all other components had been mixed. 10 μL of each turnover sample was transferred to a 200 μL thin-walled plastic tube (PCR tube) under a bed of N_2 vapor and immediately flash-frozen in liquid N_2. The entire process was completed within 15 seconds (from the initiation of turnover to freezing). Frozen turnover samples were stored under liquid N_2 until grid preparation.

Turnover samples contained a final concentration of 6 μM MoFeP, 60 μM FeP (except for the MoFeP control sample, which did not contain FeP), 5 mM $MgCl_2$, 5 mM Na_2ATP, 5 mM NaDT, 20 mM Tris, pH 8.0, and 25 mM NaCl. In addition, the BeF_x-inhibited sample contained 25 mM NaF and 5 mM $BeSO_4$. As mentioned in the text, the ATP and dithionite concentrations were chosen to ensure that they are not depleted during the 30-s sample preparation/turnover periodic while minimizing background electron scattering. We purposefully did not include an ATP regeneration mixture (creatine phosphokinase and phosphocreatine) to minimize sample heterogeneity. Given that each nitrogenase turnover cycle operates at ~1 s^{-1} under ideal conditions (*5*) (consuming 16 ATP and 8 electron equivalents) and the MoFeP concentration of 6 μM with only one of the αβ-subunits active at a time), we can calculate that at most 2.8 mM ATP and 1.4 mM electron equivalents would be consumed during 30 s.

CryoEM grid preparation

All samples were prepared on UltraAuFoil 1.2/1.3, 300 mesh grids that had been freshly plasma-cleaned using a Gatan Solarus II plasma cleaner (10 s, 15 Watts, 75% Ar/25% O_2 atmosphere). To minimize exposure to air and reaction time between thawing frozen samples and freezing grids, all grids were prepared using a custom manual plunge freezer designed by the Herzik Lab located in a humidified (≥95% relative humidity) cold room (4 ˚C). Immediately after thawing, 3 μL of the sample was applied to the grid surface followed by manual blotting for ~5 to 6 s using Whatman No. 1 filter paper before vitrifying in an 50% ethane/ 50% propane liquid mixture cooled by liquid N_2 (*37*). The time that each sample spent outside of liquid N_2 was less than 15 sec. Grids were stored under liquid N_2 until data collection. We found that this sample preparation strategy consistently afforded the formation of uniformly thin ice and largely mitigated the occurrence of preferred particle orientations at the air-water interface (which was commonly observed when using a Vitrobot for grid freezing). Importantly, the grid preparation procedure was sufficiently quick to prevent any potential O_2-based oxidative damage to component proteins, as indicated by the observation of intact FeP and reduced P-clusters in $^{t/o}$Complex-1 and $^{t/o}$Complex-2 (fig. S7). We note that the P-clusters of ^{rs}MoFeP are observed to be in the two-electron-oxidized, P^{ox} state (fig. S7), however, this does not necessarily indicate exposure to O_2 as the reduction potential of the P^{ox}/P^{N} couple is moderately high (–300 mV) (*38*). As observed in crystal structures of MoFeP (*39*, *40*), the P^{ox} state can be populated even under anaerobic conditions in the presence of dithionite whose reduction potential can vary in a condition-dependent manner (*41*).

EM data acquisition and image processing

^{rs}MoFeP: Data acquisition for the free MoFeP (^{rs}MoFeP) was carried out at UCSD's CryoEM Facility on a Titan Krios G3 (Thermo Fisher Scientific) operating at 300 keV equipped with a Gatan BioContinuum energy filter. Images were collected at a magnification of 165,000x in EF-TEM mode (0.815 Å calibrated pixel size) on a Gatan K2 detector using a 20-eV slit width and a cumulative electron exposure of ~65 electrons/$Å^2$ (50 frames). Data were collected automatically using EPU with aberration free image shift using a defocus range of -0.5 – -2.5 μm. Motion correction was performed using the MotionCor2 frame alignment program implemented within

RELION (*42*) 4.0-beta1 using 7x7 tiled frames with a B-factor of 250. Dose-weighted images were used for preliminary processing and CTF estimation using CTFFind4 within RELION (1024-pixel box size, 0.1 amplitude contrast, 30 Å minimum resolution, 3 Å maximum resolution) (*42, 43*). Aligned images with a CTF-estimated resolution below 5 Å or with a cumulative total motion exceeding 60 Å were excluded. For free MoFeP, initial particle picks were obtained using cryoSPARC Live's blob picker (50 – 120 Å circular and elliptical blobs) and an *ab initio* model was generated using optimal 2-D classes (*44*). This initial model was then used to generate 2-D templates for automated template-based particle picking using RELION 4.0-beta2 (*38*). A total of (1,527,385+1,508,038) particle picks were extracted from (1,587+2,337) micrographs collected across two different sessions from two different grids, downsampled 4 x 4 (3.26 Å/pixel, 64 pixel box size) and subjected to iterative rounds of reference-free 2-D classification (100 classes, tau_fudge=1, VDAM, ignore first CTF peak, 140 Å mask). Particles were subjected to four iterative rounds of 2-D classification and those 2-D class averages containing the strongest secondary structural details were isolated (1,497,616 particles in total) for 3-D auto-refinement using C_1 symmetry (*45*). Each session was then processed in parallel. The refined coordinates were used to re-center and re-extract particles unbinned (0.815 Å/pixel, 384 pixel box size). These particles were refined against a scaled version of the previously refined map followed by CTF refinement (per-particle defocus UV, per-micrograph astigmatism, anti-symmetrical and symmetrical higher-order aberrations). Following an iterative rounds of 3-D and CTF refinement, particles were subjected to RELION's Bayesian particle polishing using parameters trained against the data (--s_vel 1.52100 --s_div 15030.00000 --s_acc 2.35500) (*38*). Following particle polishing, 3-D auto-refinement, and CTF-refinement, a 2.12 Å structure was obtained. These particles were then subjected to a no-alignment 3-D classification (8 classes, tau_fudge=2) and the best classes (167,110 and 214,991 particles) were selected for iterative rounds of 3-D and CTF refinement followed by particle polishing using the same parameters but 512-pixel extraction box size. Both sessions were then combined and a 3-D auto-refinement led to a to ~2.01 Å refinement. Another round of no-alignment 3-D classification was performed (6 classes, tau_fudge=8) and particles comprising the highest-quality classes (177,123 particles) were combined 3-D auto-refined and then imported into cryoSPARC for a non-uniform refinement using C_1 symmetry (1.91 Å resolution) or C_2 symmetry (1.81 Å resolution) (*44*).

$^{t/o}$Complex-1 and $^{t/o}$Complex-2: Data for the nitrogenase turnover sample were collected at the S^2C^2 Stanford-SLAC CryoEM Center on TEM Gamma (Titan Krios G3i (Thermo Fisher Scientific) equipped with a Gatan K3 direct electron detector) operating at 300 keV. Images were collected at a magnification of 135,000x (0.835 Å/pixel) on a K3 detector with an electron exposure of ~65 electrons/Å^2 (66 frames) with a nominal defocus range of -1.2 – -2.0 µm. Motion correction was performed using the MotionCor2 frame alignment program implemented within RELION 4.0-beta1 using 10x14 tiled frames with a B-factor of 250 (*42, 43*). Dose-weighted images were used for preliminary processing and CTF estimation using CTFFind4 within RELION (1024-pixel box size, 0.1 amplitude contrast, 30 Å minimum resolution, 3 Å maximum resolution) (*38, 42*). Aligned images with a CTF-estimated resolution below 5 Å or with a cumulative total motion exceeding 60 Å were excluded. The resting state MoFeP structure was used to template pick ~50 movies and the top picks were used to train crYOLO for picking against the entire data set (*47*). 19,711,170 picks were obtained from 14,903 micrographs and extracted in RELION 4.0-beta2 downsampled 8 x 8 (6.68 Å/pixel, 64 pixel box size), randomly split into ~1M particle sets, and each subjected to iterative rounds of reference-free 2-D classification (200 classes,

tau_fudge=1, VDAM, ignore first CTF peak, 180 Å mask) where only obvious false classes were eliminated (*42*). 11,955,963 particles were then re-centered and re-extracted, downsampled 4 x 4 (3.34 Å/pixel, 96 pixel box size), randomly split into ~1M particle sets and each subjected to iterative rounds of reference-free 2-D classification (200 classes, tau_fudge=1, VDAM, ignore first CTF peak, 180 Å mask) where only obvious false classes were eliminated. 7,708,206 particles from the best classes were combined, randomly split into 10 subsets, and subjected to another round of 2-D classification. The best nitrogenase classes were then set aside and the remaining classes were re-ran through 2-D classification. The best nitrogenase classes were then combined with the previous run and subjected to 3-D auto-refine. These particles were then re-centered and re-extracted downsampled 4 x 4 (3.34 Å/pixel, 96 pixel box size) with duplicates removed. 4,121,671 particles were imported into cryoSPARC v3.3.2 and subjected to a heterogeneous refinement using four nitrogenase 1:1 classes and one 20S proteasome class (EMDB-8741) (*44*). The best 1:1 nitrogenase class comprising 2,511,497 particles was then subjected to a 2-class heterogenous refinement using 1:1 nitrogenase and MoFeP volumes as initial models. 1:1 complexes and MoFeP particles were then re-ran through this 2-class heterogenous refinement two times before combining all the 1:1 complexes and MoFeP particles separately and subjected to a non-uniform Refinement. These particles were then re-centered and re-extracted in RELION downsampled 2 x 2 (1.67 Å/pixel, 192 pixel box size) with duplicates removed (*42*). 906,326 1:1 complex particles were subjected to a non-uniform refinement in cryoSPARC yielding a Nyquist-limited 3.43 Å resolution map with high-quality FeP density. These particles were then subjected to a 3-D variability analysis (two modes, four intermediate clusters, 5 Å low-pass, no overlap) (*48*). The best 1:1 nitrogenase class was then subjected to another round of non-uniform refinement and 3-D variability analysis (two modes, four intermediate clusters, 5 Å low-pass filter) (*48*). Each cluster was then independently subjected to non-uniform refinement and the best two classes with FeP density for both subunits were re-centered, re-extracted in RELION without downsampling (0.835 Å/pixel, 384 pixel box size) and 3-D auto-refined followed by Bayesian particle polishing using parameters trained against the data (--s_vel 0.9225 --s_div 6570.00000 --s_acc 2.65500) (*38*). These particles were then imported into cryoSPARC for a non-uniform refinement, yielding 2.38 Å and 2.34 Å resolution maps for the ATP-ATP and ATP/ADP-ADP structures, respectively (*44*). A soft mask for FeP was then used for a local refinement (4-Å deviation over priors, 4-degree search, 4-Å shift search) yielding 2.75 Å and 3.01 Å maps for the ATP-ATP and ATP/ADP-ADP structures, respectively. The composite half maps from each independent half set from full and locally refined were assembled (maximum voxel value) and subjected to deepEMhancer (*49*) (high-resolution model; version 0.13). The FSC estimated resolution for the composite maps were 2.28 Å and 2.29 Å for the ATP-ATP and ATP/ADP-ADP complex structures, respectively.

BeFx-trapped nitrogenase complex: Data for the BeF_x-trapped complex were collected at UCSD's CryoEM Facility on a Titan Krios G3 (Thermo Fisher Scientific) operating at 300 keV equipped with a Gatan BioContinuum energy filter. Images were collected at a magnification of 165,000x in EF-TEM mode (0.815 Å calibrated pixel size) on a Gatan K2 detector using a 20-eV slit width and a cumulative electron exposure of ~65 electrons/$Å^2$ (50 frames). Data were collected automatically using EPU with aberration free image shift using a defocus range of -0.5 – -2.5 µm. 4 separate data sets were collected using 0˚, 15˚ or 25˚ specimen tilt. Motion correction was performed using the MotionCor2 frame alignment program implemented within RELION 4.0-beta1 using 7x7 tiled frames with a B-factor of 250 (*43*). Dose-weighted images were used for preliminary processing and CTF estimation using CTFFind4 within RELION (1024-pixel box size,

0.1 amplitude contrast, 30 Å minimum resolution, 3 Å maximum resolution) (*42*). Aligned images with a CTF-estimated resolution below 5 Å or with a cumulative total motion exceeding 60 Å were excluded. Initial particle picks were obtained using RELION's template picker using free MoFeP as a template (*42*). A total of (271,261+165,767+349+541+330,486) particle picks were extracted from (2,085+1,718+2,211+2,099) micrographs collected across four different sessions from two different grids, downsampled 8 x 8 (6.52 Å/pixel, 48 pixel box size). Each data set was subjected to two rounds of reference-free 2-D classification (50 classes, tau_fudge=1, VDAM, ignore first CTF peak, 220 Å mask). Particles from 2-D class averages containing the strongest secondary structural details (148,743+95,336+163,920+91,161 particles) were combined and subjected to another round of 2-D classification (50 classes, tau_fudge=1, VDAM, ignore first CTF peak, 220 Å mask). 424,249 particles were 3-D auto-refined (C_1 symmetry), re-centered and re-extracted (removing duplicates) without downsampling (0.815 Å/pixel, 384 pixel box size). The particles were then 3-D auto-refined and subjected to Bayesian particle polishing using parameters determined from the free MoFeP data set. These particles then underwent 3-D auto-refinement, CTF refinement (defocus UVA and aberrations), and a 3-D auto-refinement before a no-alignment 3-D classification (8 classes, tau_fudge=8). The best classes (397,392 particles) were then refined followed by local FeP masked 3-D classification (8 classes, tau_fudge=2). 2:1 complex particles were separated and 3-D refined followed by a subsequent no-alignment 3-D classification (4 classes, tau_fudge=24). The three best classes, representing 72,125 particles, were then subjected to 3-D autorefinement, CTF refinement, and a 3-D auto-refinement particles were subjected to Bayesian particle polishing using parameters determined from this data set (--s_vel 1.3275 --s_div 5955.00000 --s_acc 1.63500). A final series of 3-D auto-refinement, CTF refinement, and 3-D auto-refinement yielded a 2.40 Å resolution structure for the 2:1 BeF_x-trapped FeP:MoFeP complex.

Local resolution estimates were performed using cryoSPARC (*44*). 3-D FSC calculations were performed using the 3-DFSC server. Visualization was performed using UCSF's Chimera and ChimeraX. Particle meta data manipulation was performed using csparc2star.py and in-house developed Python scripts.

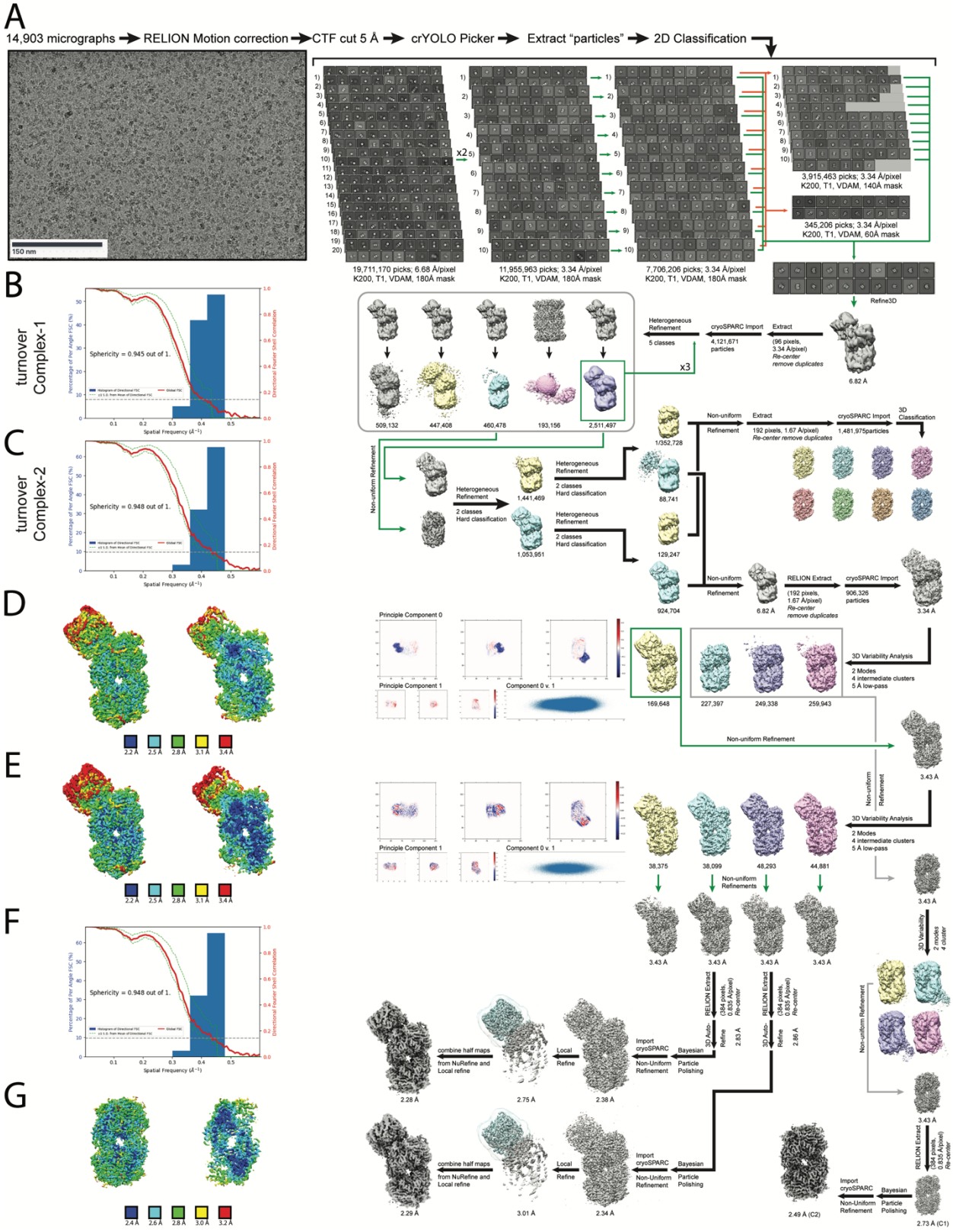
A
14,903 micrographs
RELION Motion correction
CTF cut 5 Å
crYOLO Picker
Extract "particles"
2D Classification
150 nm
19,711,170 picks; 6.68 Å/pixel
K200, T1, VDAM, 180Å mask
11,955,963 picks; 3.34 Å/pixel
K200, T1, VDAM, 180Å mask
7,706,206 picks; 3.34 Å/pixel
K200, T1, VDAM, 180Å mask
3,915,463 picks; 3.34 Å/pixel
K200, T1, VDAM, 140Å mask
345,206 picks; 3.34 Å/pixel
K200, T1, VDAM, 60Å mask
Refine3D
B
turnover Complex-1
Sphericity = 0.945 out of 1.
C
turnover Complex-2
Sphericity = 0.948 out of 1.
Spatial Frequency (Å⁻¹)
Percentage of Per Angle FSC (%)
Directional Fourier Shell Correlation
Heterogeneous Refinement
5 classes
cryoSPARC Import
4,121,671 particles
Extract
(96 pixels, 3.34 Å/pixel)
Re-center
remove duplicates
x3
6.82 Å
509,132
447,408
460,478
193,156
2,511,497
Non-uniform Refinement
2 classes Hard classification
1,441,469
1,053,951
1/352,728
88,741
129,247
924,704
Non-uniform Refinement
Extract
192 pixels, 1.67 Å/pixel)
Re-center remove duplicates
cryoSPARC Import
1,481,975particles
3D Classification
RELION Extract
(192 pixels, 1.67 Å/pixel)
Re-center
remove duplicates
cryoSPARC Import
906,326 particles
3.34 Å
D
E
F
G
2.2 Å
2.5 Å
2.8 Å
3.1 Å
3.4 Å
2.4 Å
2.6 Å
2.8 Å
3.0 Å
3.2 Å
Principle Component 0
Principle Component 1
Component 0 v. 1
169,648
227,397
249,338
259,943
3D Variability Analysis
2 Modes
4 intermediate clusters
5 Å low-pass
Non-uniform Refinement
3.43 Å
38,375
38,099
48,293
44,881
Non-uniform Refinements
combine half maps
from NuRefine and Local refine
Local Refine
Import cryoSPARC Non-Uniform Refinement
Bayesian Particle Polishing
3D Auto Refine
RELION Extract
(384 pixels, 0.835 Å/pixel)
Re-center
2.83 Å
2.86 Å
2.28 Å
2.75 Å
2.38 Å
2.29 Å
3.01 Å
2.34 Å
2.49 Å (C2)
2.73 Å (C1)

Fig. S1. Data processing flowchart for the single-particle cryoEM analysis of nitrogenase complexes formed under turnover. (A) Representative motion-corrected micrograph of vitrified nitrogenase collected at ~1.5 μm underfocus. 19,711,170 particles were identified from dose-weighted micrographs by crYOLO trained using resting state MoFeP. These particles were extracted and downsampled 8 x 8 in RELION, randomly split into ~1M particle sets, and subjected to iterative rounds of reference-free 2-D classification in RELION. Representative 2-D class averages are shown for each iterative step. The best nitrogenase classes were set aside (green arrows) while the remaining classes were randomly split into 10 subsets and subjected to another round of 2-D classification (orange arrows). The best classes were then combined and 3-D auto-refined to 6.82 Å. Particles were then imported into cryoSPARC and subjected to a 5-class heterogenous refinement. The best class for the 1:1 nitrogenase complex was selected (green box) and two iterative rounds of two class heterogenous refinements were performed. 1:1 FeP:MoFeP complex particles were isolated and re-extracted in RELION and imported into cryoSPARC for 3-D variability analysis. The cluster with the strongest FeP density in the 1:1 FeP:MoFeP complex was selected (green box) and non-uniform refined before a final round of 3-D variability analysis. The two clusters with density for both proteins were re-centered and re-extracted in RELION without downsampling, 3-D auto-refined, and subjected to Bayesian particle polishing. After polishing, the particles were imported into cryoSPARC and locally refined. The half maps were combined, resulting in the $^{t/o}$Complex-1 and $^{t/o}$Complex-2 resolving to 2.28 Å and 2.29 Å, respectively. Histogram and directional 3-D FSC plots generated from the independent composite half maps contributing to the ~2.28 Å and 2.29 Å resolution **(B)** $^{t/o}$Complex-1 and **(C)** $^{t/o}$Complex-2 structures, respectively. **(D)** EM density of $^{t/o}$Complex-1 colored by local resolution. The left image corresponds to the surface of $^{t/o}$Complex-1, and the right image is a cross-section of the complex. **(E)** EM density of $^{t/o}$Complex-2 colored by local resolution. The left image corresponds to the surface of $^{t/o}$Complex-2, and the right image is a cross-section of the complex. **(F)** Histogram and directional 3-D FSC plots generated from the independent composite half maps contributing to the ~2.59 Å resolution MoFeP (C_2 symmetry) map. **(G)** EM density of MoFeP (C_2 symmetry) colored by local resolution. The left image is surface view of MoFeP, and the right image is a cross-section of the protein.

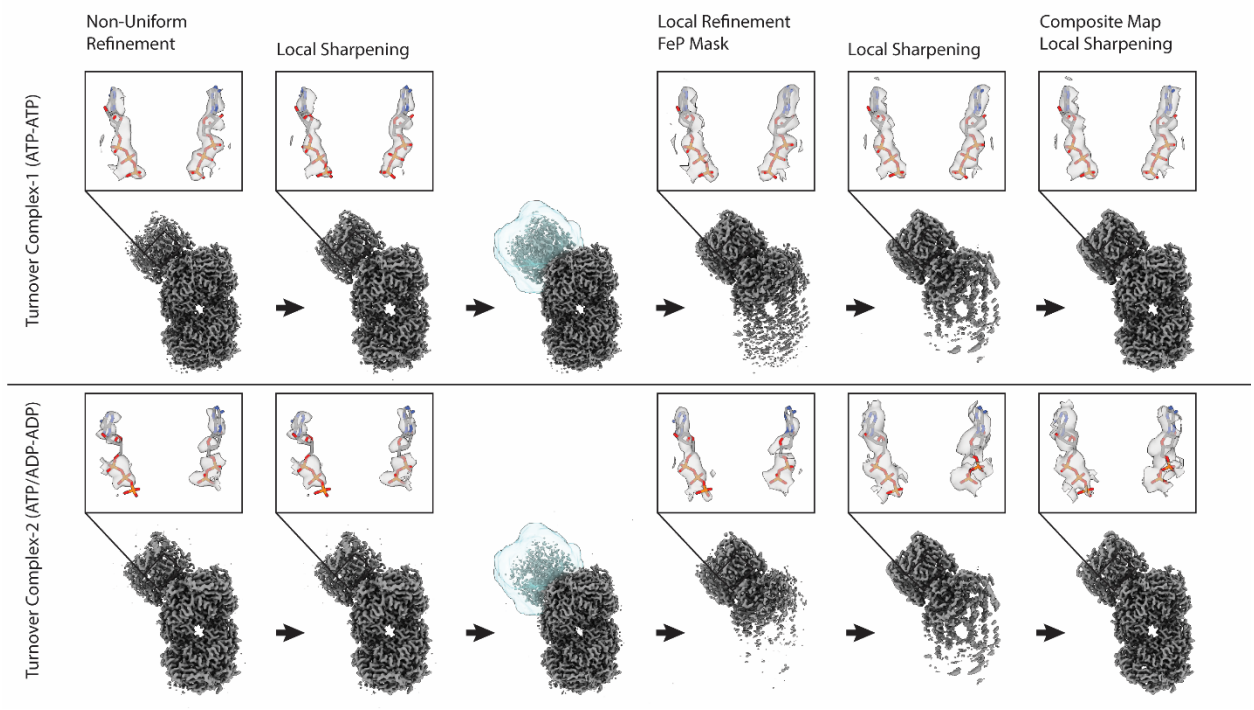

Figure S2. Improvements in map quality for the 1:1 FeP:MoFeP complexes formed under turnover. (left to right) Non-uniform refinements of the $^{t/o}$Complex-1 (top) and $^{t/o}$Complex-2 (bottom) yielded ~2.4 Å resolution maps with lower resolution regions for the FeP subunits. Local noise estimates and sharpening using deepEMhancer were used to improve the quality of the FeP density. Local refinement of each particle set using a soft FeP protein mask and subsequent local sharpening improved the EM density quality for the FeP subunits with lower quality density for the MoFeP subunits. Maximal voxel values for the non-uniform and local refinements were taken to generate composite half maps that were then used for resolution estimation, local noise estimates and sharpening.

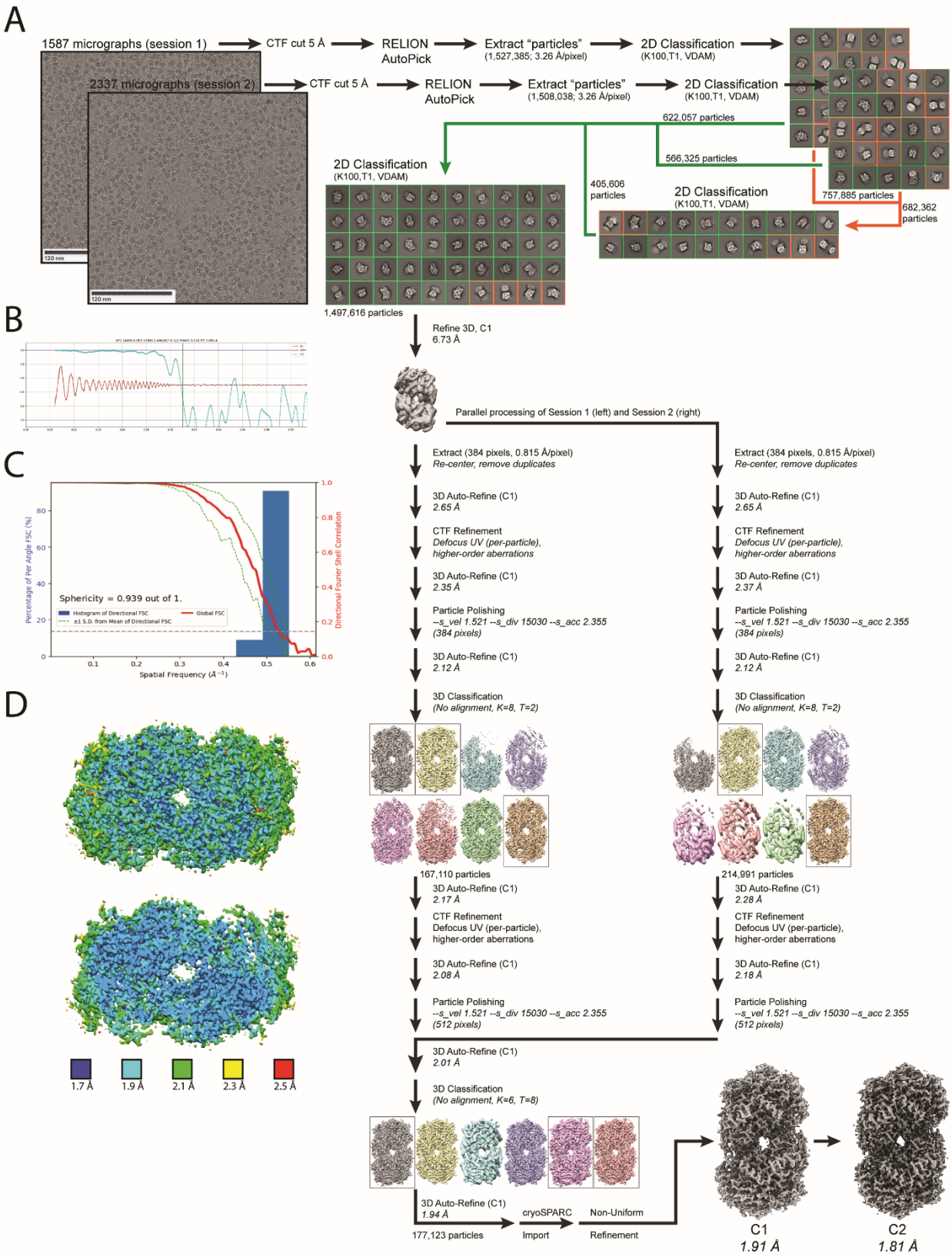
A
1587 micrographs (session 1)
CTF cut 5 Å
RELION AutoPick
Extract "particles" (1,527,385; 3.26 Å/pixel)
2D Classification (K100,T1, VDAM)
2337 micrographs (session 2)
CTF cut 5 Å
RELION AutoPick
Extract "particles" (1,508,038; 3.26 Å/pixel)
2D Classification (K100,T1, VDAM)
622,057 particles
566,325 particles
757,885 particles
682,362 particles
405,606 particles
2D Classification (K100,T1, VDAM)
2D Classification (K100,T1, VDAM)
1,497,616 particles
B
Refine 3D, C1 6.73 Å
Parallel processing of Session 1 (left) and Session 2 (right)
C
Sphericity = 0.939 out of 1.
Histogram of Directional FSC
Global FSC
±1 S.D. from Mean of Directional FSC
Percentage of Per Angle FSC (%)
Directional Fourier Shell Correlation
Spatial Frequency (Å⁻¹)
Extract (384 pixels, 0.815 Å/pixel)
Re-center, remove duplicates
3D Auto-Refine (C1)
2.65 Å
CTF Refinement
Defocus UV (per-particle), higher-order aberrations
3D Auto-Refine (C1)
2.35 Å
Particle Polishing
--s_vel 1.521 --s_div 15030 --s_acc 2.355
(384 pixels)
3D Auto-Refine (C1)
2.12 Å
3D Classification
(No alignment, K=8, T=2)
167,110 particles
214,991 particles
3D Auto-Refine (C1)
2.17 Å
2.28 Å
CTF Refinement
Defocus UV (per-particle), higher-order aberrations
3D Auto-Refine (C1)
2.08 Å
2.18 Å
Particle Polishing
--s_vel 1.521 --s_div 15030 --s_acc 2.355
(512 pixels)
3D Auto-Refine (C1)
2.01 Å
3D Classification
(No alignment, K=6, T=8)
3D Auto-Refine (C1)
1.94 Å
177,123 particles
cryoSPARC Import
Non-Uniform Refinement
C1
1.91 Å
C2
1.81 Å
D
1.7 Å
1.9 Å
2.1 Å
2.3 Å
2.5 Å

Fig. S3. Data processing flowchart for the single-particle cryo-EM analysis of free MoFeP (^{rs}MoFeP). (A) Representative motion-corrected micrographs of vitrified MoFeP collected at ~1.5 µm underfocus. ~1.5M particles were identified using RELION's automated template based Autopicking, downsampled 8 x 8, and subjected to iterative rounds of reference free 2-D classification. Classes with strong secondary structural detail were isolated (green boxes/arrows), while poorly aligning classes were subjected to a final round of 2-D classification (orange boxes/arrows). All good classes were combined for an initial round of 3-D auto-refinement that refined to 6.73 Å resolution. Particles were then split into their respective sessions and processed in parallel. The refined coordinates were used to re-center and re-extract particles without binning and subjected to 3-D auto-refinement, CTF refinement, and 3-D auto-refinement before Bayesian particle polishing in RELION. No alignment 3-D classification was performed, and the best classes were selected (boxed). After iterative rounds of refinement, the sessions were combined, imported into cryoSPARC for non-uniform refinement in C_1 or C_2 symmetries using defocus and aberration refinement to yield 1.91 Å (C_1) and 1.81 Å (C_2) resolution structures. **(B)** Representative 2-D CTF fit for the data. **(C)** Histogram and directional 3-D FSC (*50*) plots generated from the independent half maps contributing to the ~1.81 Å C_2 structure. **(D)** EM density of the C_2-refined structure colored by local resolution. The top image corresponds to the surface of MoFeP and the bottom image corresponds to a cross-section of the protein, highlighting core regions.

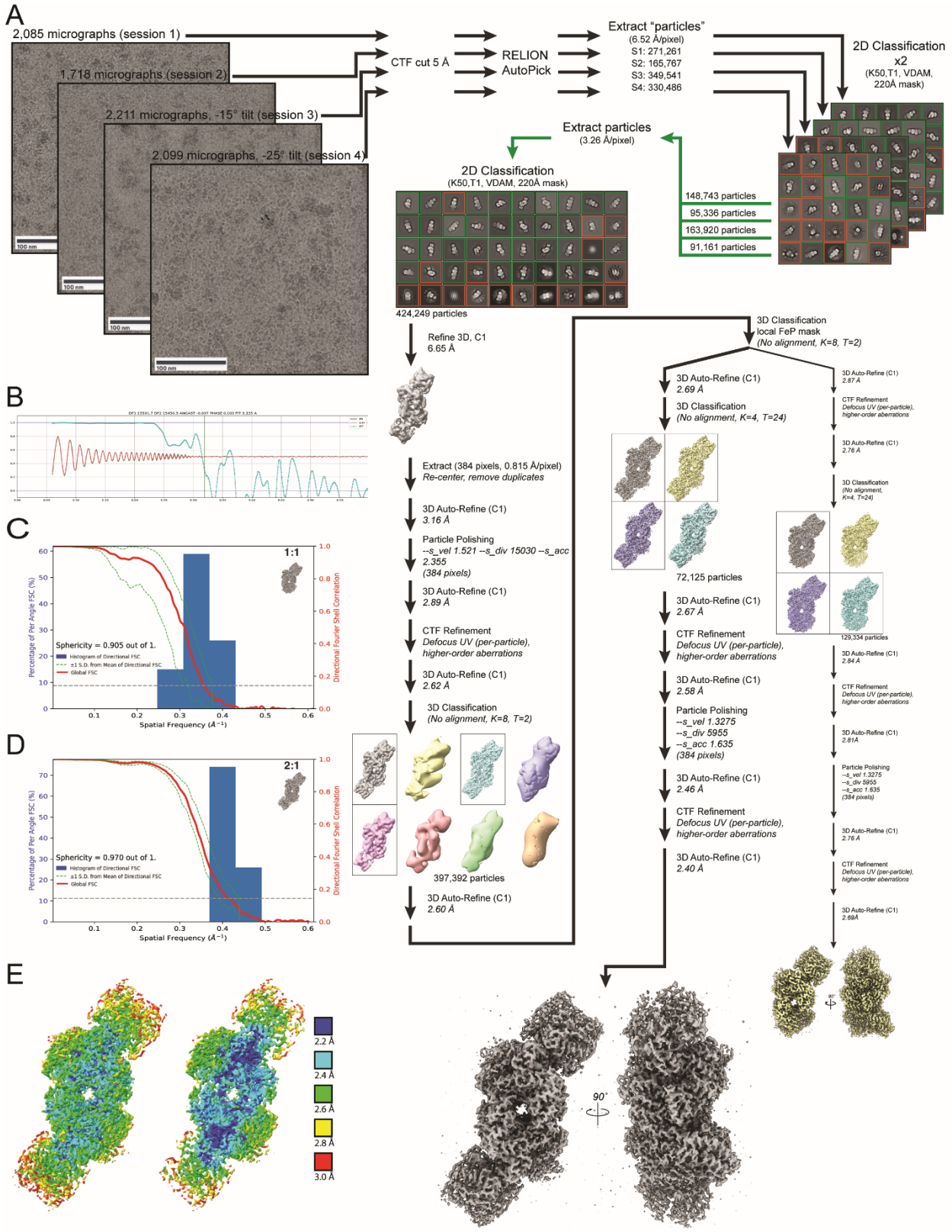
A
2,085 micrographs (session 1)
1,718 micrographs (session 2)
2,211 micrographs, -15° tilt (session 3)
2,099 micrographs, -25° tilt (session 4)
CTF cut 5 Å
RELION AutoPick
Extract "particles"
(6.52 Å/pixel)
S1: 271,261
S2: 165,767
S3: 349,541
S4: 330,486
2D Classification x2
(K50,T1, VDAM, 220Å mask)
Extract particles
(3.26 Å/pixel)
2D Classification
(K50,T1, VDAM, 220Å mask)
148,743 particles
95,336 particles
163,920 particles
91,161 particles
424,249 particles
Refine 3D, C1
6.65 Å
B
C
D
E
Extract (384 pixels, 0.815 Å/pixel)
Re-center, remove duplicates
3D Auto-Refine (C1)
3.16 Å
Particle Polishing
--s_vel 1.521 --s_div 15030 --s_acc 2.355
(384 pixels)
3D Auto-Refine (C1)
2.89 Å
CTF Refinement
Defocus UV (per-particle), higher-order aberrations
3D Auto-Refine (C1)
2.62 Å
3D Classification
(No alignment, K=8, T=2)
397,392 particles
3D Auto-Refine (C1)
2.60 Å
3D Classification
local FeP mask
(No alignment, K=8, T=2)
3D Auto-Refine (C1)
2.69 Å
3D Classification
(No alignment, K=4, T=24)
72,125 particles
3D Auto-Refine (C1)
2.67 Å
CTF Refinement
Defocus UV (per-particle), higher-order aberrations
3D Auto-Refine (C1)
2.58 Å
Particle Polishing
--s_vel 1.3275
--s_div 5955
--s_acc 1.635
(384 pixels)
3D Auto-Refine (C1)
2.46 Å
CTF Refinement
Defocus UV (per-particle), higher-order aberrations
3D Auto-Refine (C1)
2.40 Å
3D Auto-Refine (C1)
2.87 Å
CTF Refinement
Defocus UV (per-particle), higher-order aberrations
3D Auto-Refine (C1)
2.76 Å
3D Classification
(No alignment, K=4, T=24)
129,334 particles
3D Auto-Refine (C1)
2.84 Å
CTF Refinement
Defocus UV (per-particle), higher-order aberrations
3D Auto-Refine (C1)
2.81Å
Particle Polishing
--s_vel 1.3275
--s_div 5955
--s_acc 1.635
(384 pixels)
3D Auto-Refine (C1)
2.76 Å
CTF Refinement
Defocus UV (per-particle), higher-order aberrations
3D Auto-Refine (C1)
2.69Å
1:1
Sphericity = 0.905 out of 1.
Histogram of Directional FSC
±1 S.D. from Mean of Directional FSC
Global FSC
Percentage of Per Angle FSC (%)
Directional Fourier Shell Correlation
Spatial Frequency (Å⁻¹)
2:1
Sphericity = 0.970 out of 1.
2.2 Å
2.4 Å
2.6 Å
2.8 Å
3.0 Å
90°

Fig. S4. Data processing flowchart for the single-particle cryo-EM analysis of the BeFx-trapped nitrogenase complex. (**A**) Representative motion-corrected micrograph for each of the datasets for vitrified BeF_x-trapped nitrogenase complexes collected at ~1.5 μm underfocus. A total of 1,117,055 particles identified from dose-weighted micrographs using RELION auto-pick with resting state MoFeP as a template. Particles were extracted from each dataset downsampled 4 x 4 and subjected to iterative rounds of 2-D classification in parallel before being combined for additional 2-D classification and 3-D auto-refinement. Particles were then re-centered and re-extracted unbinned and subjected to iterative rounds of 3-D auto- and CTF refinement, followed by a no alignment 3-D classification. The best classes were combined and subjected to additional rounds of no-alignment classification using a soft mask for the FeP subunits. 1:1 and 2:1 FeP:MoFeP complexes were separated and processed in parallel. After iterative rounds of 3-D auto- and CTF refinement, Bayesian particle polishing, ~2.69 Å and ~2.40 Å resolution structures were obtained for the 1:1 and 2:1 complexes, respectively. (**B**) Representative 2-D CTF fit for the data. (**C-D**) Histogram and directional 3-D FSC plots (*50*) generated from the independent half maps contributing to the structures of the (**C**) 1:1 and (**D**) 2:1 complexes (**E**) EM density for the 2:1 BeF_x-trapped FeP:MoFeP complex colored by local resolution. The left image shows the surface of the complex and the right image is a volume cross-section highlighting core regions.

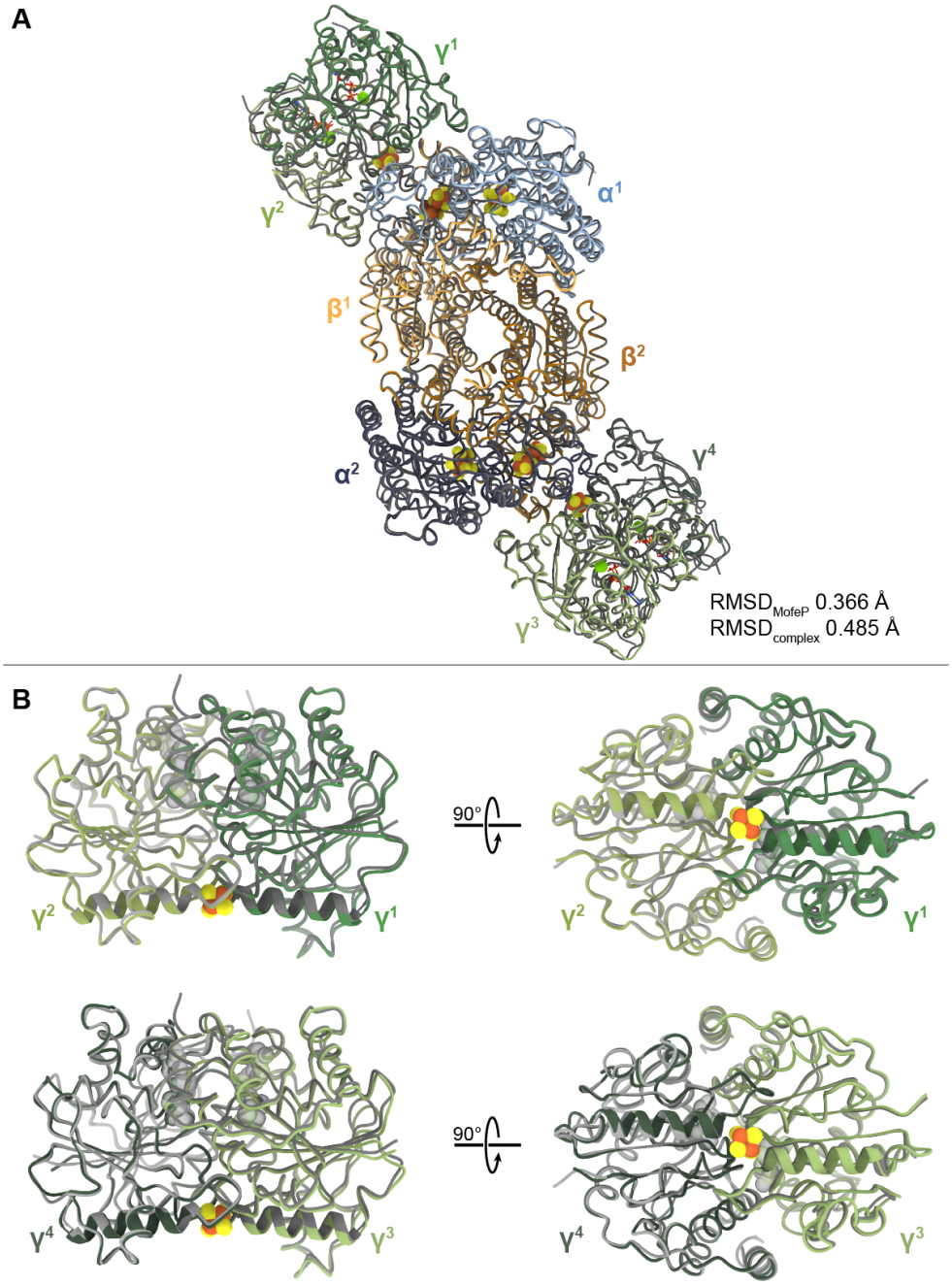

Fig. S5. Comparison of BeF_X-bound cryoEM structure with AlF_X crystal structure. (**A**) Overlay of BeF_X-trapped cryoEM structure (green, orange, and blue) with the AlF_X-trapped crystal structure (PDB ID: 1M34) (*11*) highlighting their overall similarities. Root-mean-square-deviations (RMSDs) based on all Cα positions in MoFeP and the entire complex are 0.366 Å and 0.485 Å, respectively. (**B**) Structural overlay of the FeP components (γ^1 and γ^2 top, (γ^3 and γ^4 bottom) in BeF_X- and AlF_X- trapped complexes, in which the left subunit (γ^2 or γ^4) has been aligned. The γ100's helices (residues γ98-γ112) are depicted as ribbons.

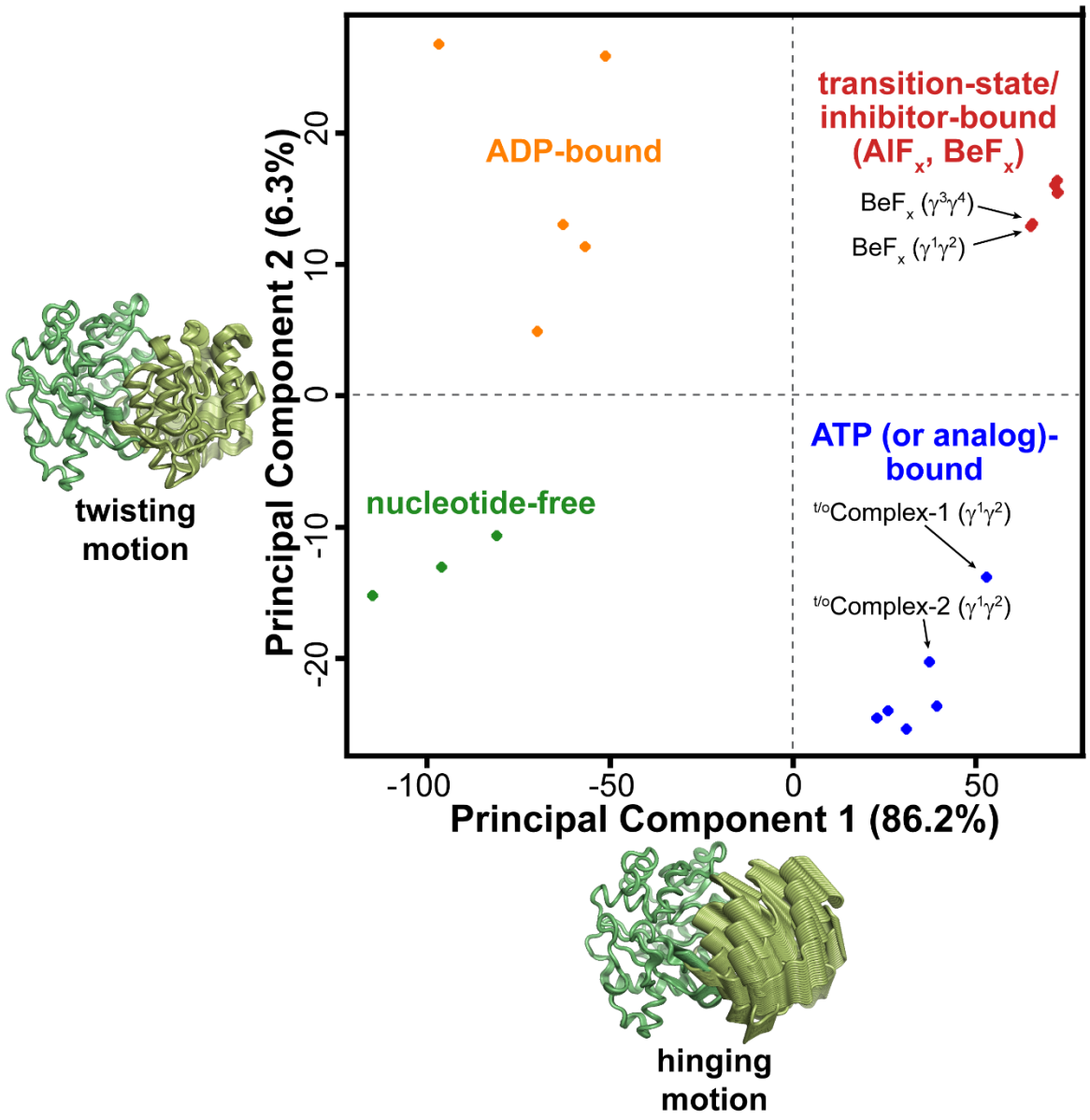

Fig. S6. Principal component analysis (PCA) of FeP. PCA of FeP was carried out using twenty available free- or MoFeP-complexed FeP structures based on prior X-ray crystallographic or current cryoEM characterization. The first two principal components (PC) account for 92.5% of the variance. PC1 and PC2 are described by the hinging/rotation and twisting motions of the two γ-subunits with respect to one another. FeP conformations clustered into four nucleotide-state-dependent classes. FeP structures from the cryoEM structures indicated with arrows.

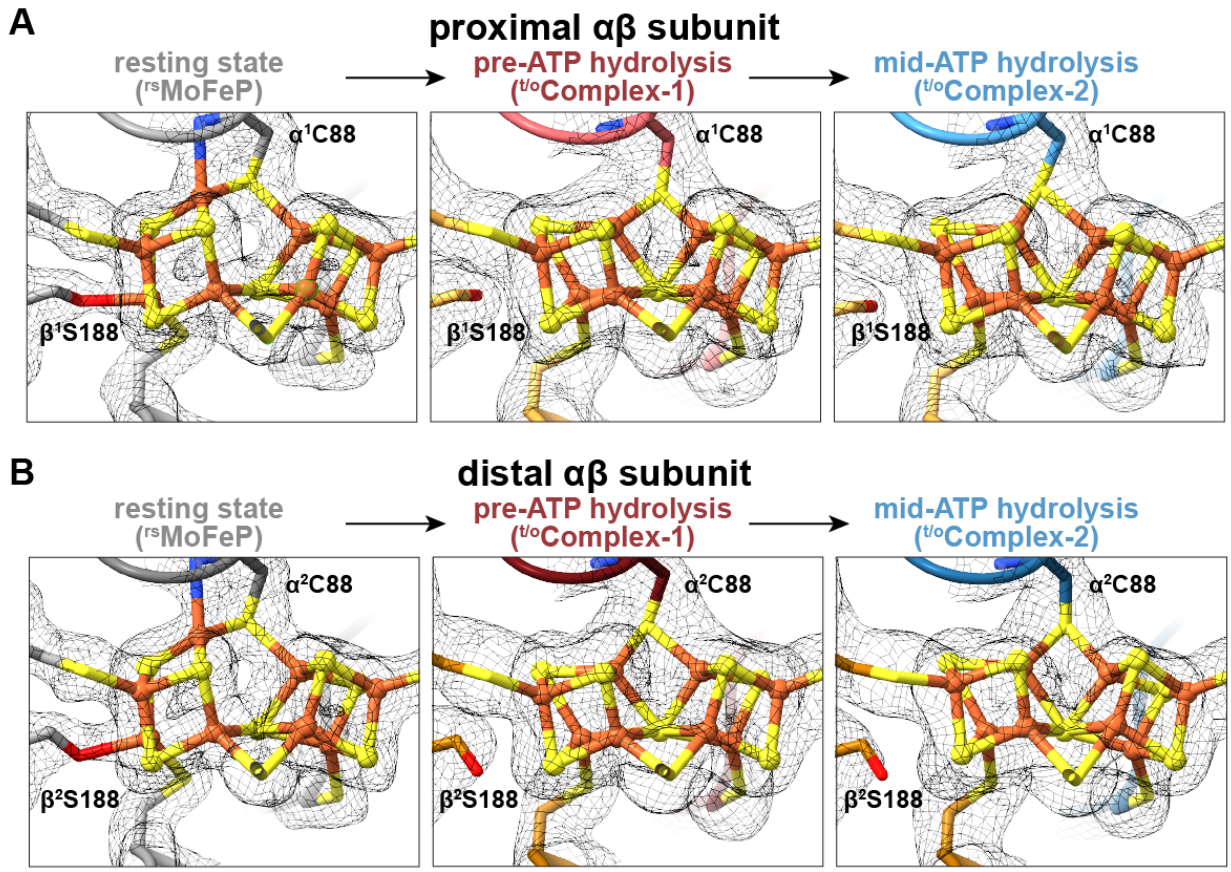

Fig. S7. P-clusters of ^{rs}MoFeP, $^{t/o}$Complex-1, and $^{t/o}$Complex-2. (**A**,**B**) Views of the P-cluster and P-cluster ligands in the proximal (**A**) and distal (**B**) αβ halves of MoFeP in ^{rs}MoFeP (gray), $^{t/o}$Complex-1 (maroon), and $^{t/o}$Complex-2 (blue) structures. CryoEM maps for each individual structure are shown as a gray mesh and contoured at the following levels: ^{rs}MoFeP – 0.008. $^{t/o}$Complex-1 – 0.065, $^{t/o}$Complex-2 – 0.075. Based on the following bond distances, we assign the P-clusters in the ^{rs}MoFeP to be in the two-electron oxidized P^{ox} state and those in the $^{t/o}$Complexes to be in the all-ferrous, P^{N} state: Fe6-$^{\beta Ser188}$O = 2.5 Å (^{rs}MoFeP), 3.6 Å ($^{t/o}$Complex-1), 3.7 Å ($^{t/o}$Complex-2); Fe6-S1 = 3.7 Å (^{rs}MoFeP), 2.6 Å ($^{t/o}$Complex-1), 2.7 Å ($^{t/o}$Complex-2); Fe5-S1 = 3.6 Å (^{rs}MoFeP), 2.6 Å ($^{t/o}$Complex-1), 2.6 Å ($^{t/o}$Complex-2); Fe5- $^{\alpha Cys88}$N = 2.5 Å (^{rs}MoFeP), 3.5 Å ($^{t/o}$Complex-1), 3.5 Å ($^{t/o}$Complex-2). All values are averages of the two clusters in each MoFeP.

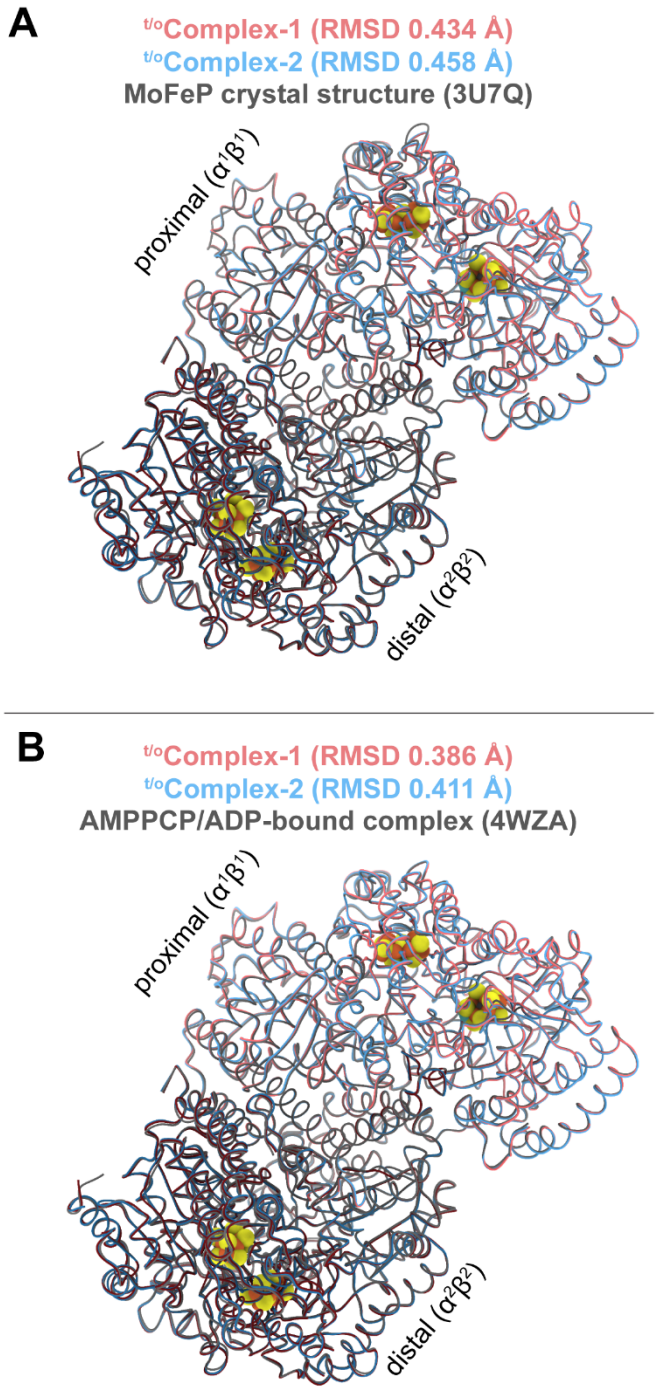

Fig. S8. Structural overlay of the MoFeP components of turnover complexes with MoFeP from previously determined crystal structures. Overlay of $^{t/o}$Complex-1 (maroon) and $^{t/o}$Complex-2 (blue) with (**A**) a crystal structure of MoFeP (gray, PDB ID: 3U7Q) (*40*), and (**B**) MoFeP from the AMPPCP/ADP bound FeP-MoFeP complex crystal structure (gray, PDB ID: 4WZA chains A,B,C,D) (*24*). Root-mean-square-deviations (RMSDs; based on all Cα positions) between the MoFeP components of the turnover complexes and those from the crystal structures are indicated.

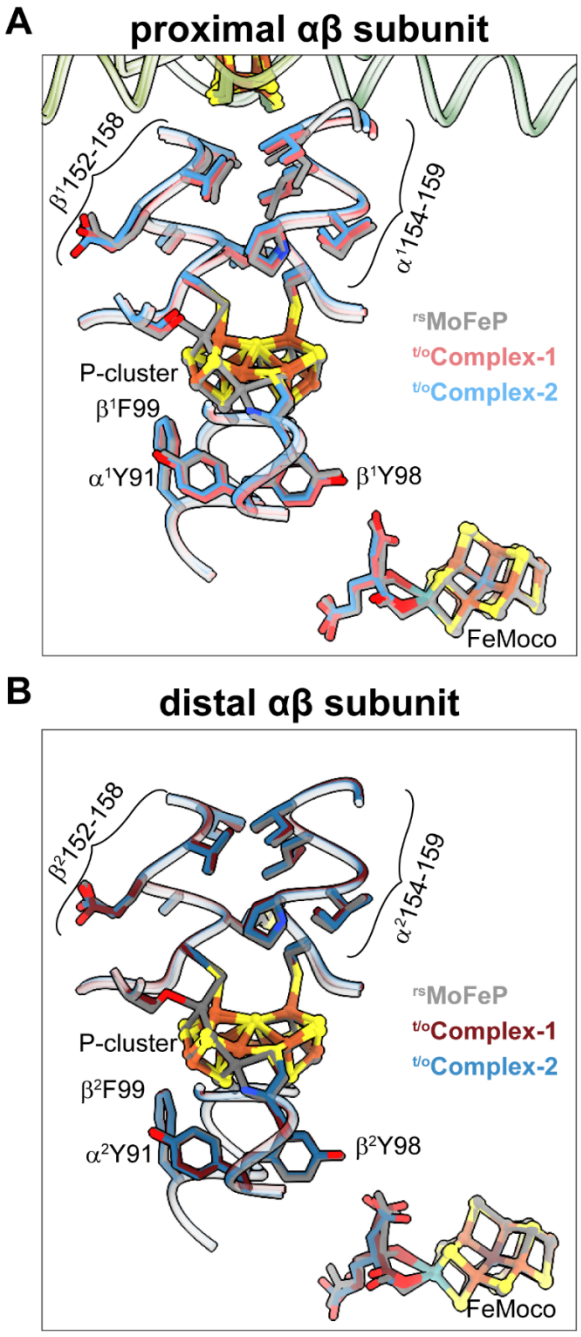

Fig. S9. Overlay of core residues along the ET pathway leading from the MoFeP surface to FeMoco. (**A**,**B**) Overlay key residues residing between the [4Fe:4S] cluster and the P-cluster, and between the P-cluster and FeMoco in ^{rs}MoFeP (gray), $^{t/o}$Complex-1 (maroon), and $^{t/o}$Complex-2 (blue) structures. The proximal (**A**) and distal (**B**) αβ halves of MoFeP are shown. γ100's helices of FeP (residues γ98-γ112) are shown in green in (**A**).

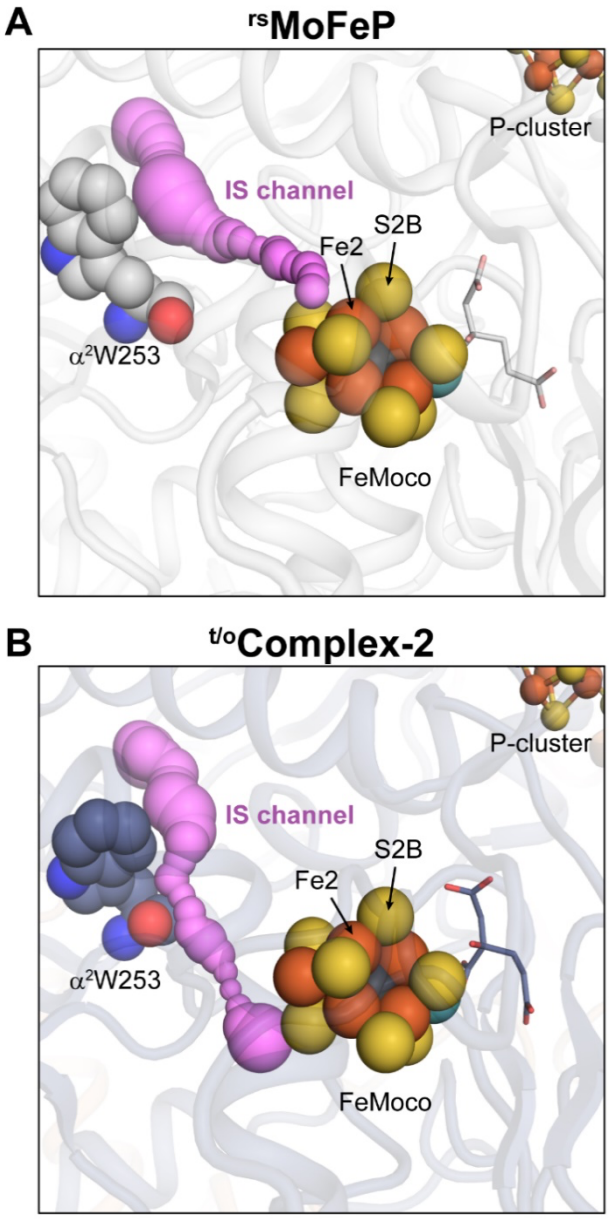

Fig. S10. Diversion of the IS channel during turnover. (**A**,**B**) The proposed substrate pathway, termed the IS channel (*28*, *51*) is shown in pink and was calculated using the software CAVER (*52*) in PyMOL (version 2.5, Schrodinger LLC). (**A**) In ^{rs}MoFeP, the IS channel leads from the surface of MoFeP to the proposed catalytic face of FeMoco. (**B**) Conformational changes during turnover, as shown in the case of $^{t/o}$Complex-2, divert the IS channel to a different face FeMoco.

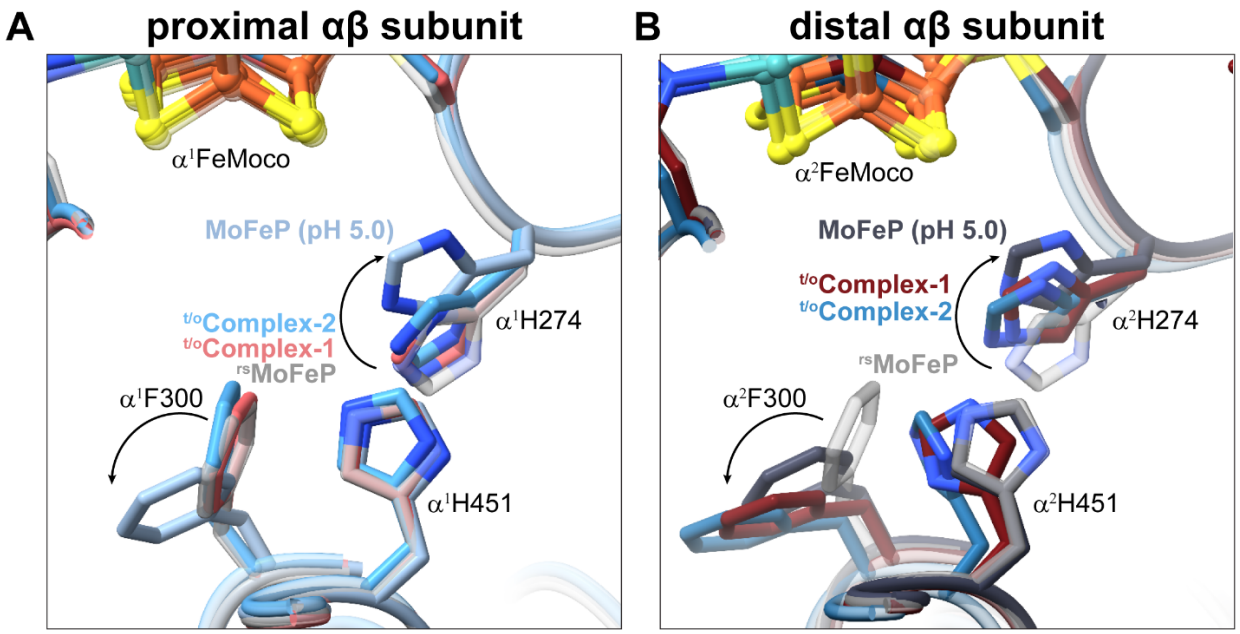

Fig. S11. Overlay of αHis274, αPhe300 and αHis451 conformations observed in nitrogenase complexes under turnover and previously determined low-pH crystal structure of MoFeP. (**A**,**B**) Overlay of the conformationally altered residues in ^{rs}MoFeP (transparent gray), $^{t/o}$Complex-1 (maroon), $^{t/o}$Complex-2 (blue), and the crystal structure of MoFeP determined at pH 5.0 (sky blue/slate PDB ID: 5VQ4) (*29*) structures in both the proximal (**A**) and distal (**B**) αβ halves of MoFeP.

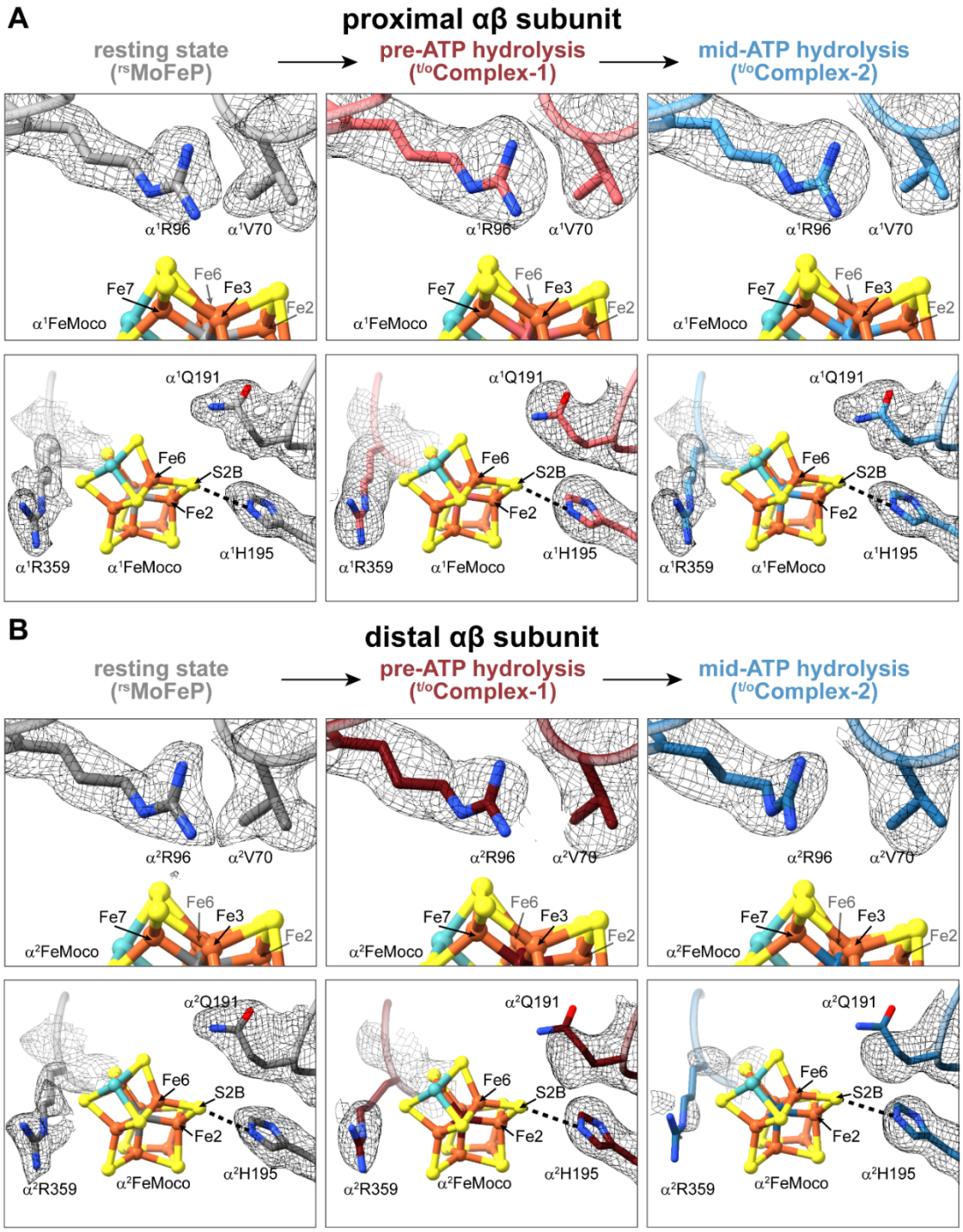

Fig. S12. The FeMoco environment in the cryoEM structures. (**A**, **B**) Views of FeMoco and the nearby residues αV70, αR96, αQ191, αH195, and αR359 in the proximal (**A**) and distal (**B**) αβ halves of MoFeP in ^{rs}MoFeP (gray), $^{t/o}$Complex-1 (maroon), and $^{t/o}$Complex-2 (blue) structures. CryoEM maps are shown as a gray mesh and contoured at the following levels: ^{rs}MoFeP – 0.008, $^{t/o}$Complex-1 – 0.065, $^{t/o}$Complex-2 – 0.075.

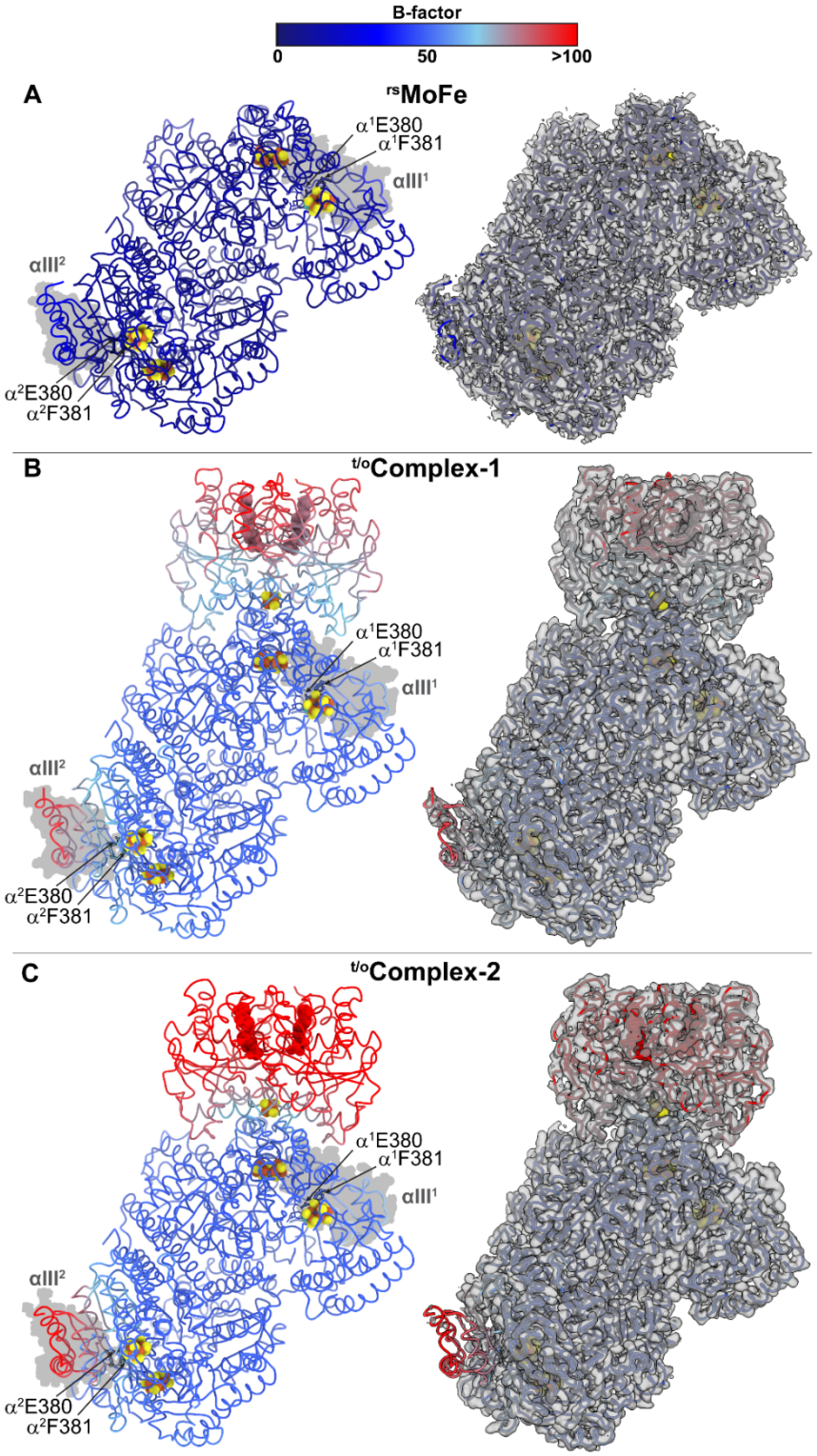

Fig. S13. $^{t/o}$Complex-1, and $^{t/o}$Complex-2 colored by B-factor and comparison of αIII densities. (**A**) ^{rs}MoFeP, (**B**) $^{t/o}$Complex-1, and (**C**) $^{t/o}$Complex-2, colored by B-factor (left) and comparison of cryoEM map densities (right).

Table S1. CryoEM data collection and refinement statistics of *Azotobacter vinelandii* $^{t/o}$Complex-1 and $^{t/o}$Complex-2.

	#1 $^{t/o}$Complex-1 (EMDB-26760) (PDB-7UT8)	**#1 $^{t/o}$Complex-2 (EMDB-26763) (PDB-7UT9)**
Data Collection	Titan Krios G3i K3 BioQuantum	
Magnification	130kx	
Voltage (kV)	300	
Spherical Aberration (mm)	2.7	
Electron Exposure ($e^-/Å^2$)	65	
Defocus range (μm)	-1.1 to -2	
Pixel size (Å, Physical/Digital)	0.835	
Energy Filter Slit Width (eV)	20	
Movies	2580	
Map Statistics and Post-Processing	$^{t/o}$Complex-1	$^{t/o}$Complex-2
Symmetry imposed	C_1	C_1
Map Resolution (Å)	2.28	2.29
Local resolution range for 75% of voxels	2.731	2.577
Local resolution range (model)	1.897 - 21.602	1.843 - 22.574
Map sharpening *B* factor ($Å^2$)	47.5	47.3
Map sharpening method	DeepEMhancer	DeepEMhancer
3-D FSC values X Y Z	 2.78 2.78 2.78	 2.66 3.28 2.66
Model Statistics and Validation	$^{t/o}$Complex-1	$^{t/o}$Complex-2
Model composition Non-hydrogen atoms Protein Nucleic acids Ligands Waters	 20223 20026 0 168 29	 20245 20021 0 164 60
B-factors ($Å^2$) Protein/Nucleic acid atoms	34.38	37.17

Ligands/non-protein atoms	43.86	51.07
R.M.S deviations Bond lengths (Å) Bond angles (˚)	 0.014 1.036	 0.013 0.993
MolProbity Score	2.09	2.07
MolProbity Clashscore	9.48	9.91
CaBLAM (% outliers)	1.51	1.27
Rotamer outliers (%)	3.43	3.20
Cis peptides (#, %)	5.6, 0.1%	5.6, 0.1%
Ramachandran Plot Favored (%) Allowed (%) Disallowed (%)	 96.91 3.05 0.04	 97.03 2.93 0.04
EM Ringer score	4.03	3.98
Map/Model FSC (0.5)	2.95	2.84

Table S2. CryoEM data collection and refinement statistics of *Azotobacter vinelandii* ^{rs}MoFeP.

	#1 ^{rs}MoFe C_1 (EMDB-26756) (PDB-7UT6)	**#1 ^{rs}MoFe C_2 (EMDB-26757) (PDB-7UT7)**
Data Collection	Titan Krios G3 K2 BioContinuum	
Magnification	165kx	
Voltage (kV)	300	
Spherical Aberration (mm)	2.7	
Electron Exposure ($e^-/Å^2$)	65	
Defocus range (μm)	-0.5 to -1.5	
Pixel size (Å, Physical/Digital)	0.815	
Energy Filter Slit Width (eV)	10	
Movies	1460 (session 1) 2313 (session 2)	
Map Statistics and Post-Processing		
Symmetry imposed	C_1	C_2
Map Resolution (Å)	1.91	1.81
Local resolution range for 75% of voxels	5.299	2.883
Local resolution range (model)	1.826 - 30.347	1.826- 29.563
Map sharpening *B* factor ($Å^2$)	37.9	39.8
Map sharpening method	DeepEMhancer	DeepEMhancer
3-D FSC values X Y Z	 2.47 2.78 2.37	 1.93 1.94 1.84
Model Statistics and Validation		
Model composition Non-hydrogen atoms Protein residues Nucleic acids Ligands Waters	 16397 15677 0 96 369	 16443 15677 0 96 415
B-factors ($Å^2$) Protein/Nucleic acid atoms Ligands/non-protein atoms	 25.30 26.66	 23.00 25.04

R.M.S deviations Bond lengths (Å) Bond angles (°)	 0.003 0.609	 0.004 0.643
MolProbity Score	1.32	1.34
MolProbity Clashscore	5.15	4.89
CaBLAM (% outliers)	0.76	0.76
Rotamer outliers (%)	0.87	0.81
Cis peptides (#, %)	6.5, 0.1%	6.5, 0.1%
Ramachandran Plot Favored (%) Allowed (%) Disallowed (%)	 97.79 2.21 0.00	 97.59 2.41 0.00
EM Ringer score	6.13	7.11

Table S3. CryoEM data collection and refinement statistics of *Azotobacter vinelandii* BeF_x trapped complex.

	#1 BeF_x trapped complex (EMDB-26764) (PDB-7UTA)	
Data Collection	Titan Krios G3 K2 BioContinuum	
Magnification	165kx	
Voltage (kV)	300	
Spherical Aberration (mm)	2.7	
Electron Exposure ($e^-/Å^2$)	65	
Defocus range (μm)	-0.5 to -1.5	
Pixel size (Å, Physical/Digital)	0.815	
Energy Filter Slit Width (eV)	10	
Movies (Tilt (°))	1460	0
	2313	0
	2211	-15
	2099	-25
Map Statistics and Post-Processing	2:1 BeF_x	
Symmetry imposed	C_1	
Map Resolution (Å)	2.40	
Local resolution range for 75% of voxels	2.883	
Local resolution range (model)	1.826- 29.563	
Map sharpening *B* factor ($Å^2$)	39.8	
Map sharpening method	DeepEMhancer	
3-D FSC values X Y Z	 3.17 2.84 2.95	
Model Statistics and Validation		
Model composition Non-hydrogen atoms Protein residues Nucleic acids	 24338 24056 0	

Ligands Waters	227 55
B-factors (Å^2) Protein/Nucleic acid atoms Ligands/non-protein atoms	 37.24 47.27
R.M.S deviations Bond lengths (Å) Bond angles (°)	 0.004 0.724
MolProbity Score	2.10
MolProbity Clashscore	11.47
CaBLAM (% outliers)	2.09
Rotamer outliers (%)	2.09
Cis peptides (#, %)	4.8, 0.1
Ramachandran Plot Favored (%) Allowed (%) Disallowed (%)	 95.89 3.98 0.13
EM Ringer score	3.87
Map/Model FSC (0.5)	2.87

Table S4. Root-mean-square-deviations (RMSDs; based on C_α positions) between various MoFeP structures.

structure	MoFeP (3u7q)	nucleotide-free complex (2afh)	AMPPCP-bound (4wzb)	ADP-bound (2afi)	AMPPCP/ADP-bound (4wza)	ADP.AlF$_x$ (1m34)	N-species-bound MoFeP (6ug0)	CO-bound MoFeP (4tkv)	^{rs}MoFeP	$^{t/o}$Complex-1	$^{t/o}$Complex-2
nucleotide-free complex (2afh)	0.365										
AMPPCP-bound (4wzb)	0.323	0.291									
ADP-bound (2afi)	0.386	0.329	0.374								
AMPPCP/ADP-bound (4wza)	0.241	0.246	0.196	0.337							
ADP.AlFx (1m34)	0.396	0.319	0.318	0.401	0.318						
N-species-bound MoFeP (6ug0)	0.232	0.324	0.283	0.328	0.283	0.378					
CO-bound MoFeP (4tkv)	0.106	0.329	0.224	0.361	0.224	0.385	0.224				
^{rs}MoFeP	0.324	0.313	0.311	0.320	0.302	0.322	0.310	0.321			
$^{t/o}$Complex-1	0.434	0.397	0.359	0.412	0.386	0.348	0.410	0.444	0.233		
$^{t/o}$Complex-2	0.458	0.416	0.385	0.420	0.411	0.375	0.436	0.465	0.246	0.170	
BeF_x-bound	0.437	0.399	0.382	0.429	0.404	0.366	0.433	0.444	0.261	0.246	0.252

Table S5. Average B-factors for the MoFeP components and the αIII domains in various nitrogenase crystal structures.

Structure (resolution / PDB ID)	average B for the entire MoFeP component (Å^2)	average B for αIII (chain A) (Å^2)	average B for αIII (chain C) (Å^2)
MoFeP with oxidized P-cluster (2.03 Å / 2 MIN)	24.13	34.70	34.14
MoFeP at pH 5.0 (2.30 Å / 5VQ4)	24.65	45.58	42.73
1.0-Å resolution MoFeP (1.0 Å / 3U7Q)	10.58	11.37	13.13
F99YMoFeP with oxidized P-cluster (1.4 Å / 6O7M)	17.08	22.62	23.09
Nucleotide-free FeP-MoFeP complex (2.1 Å / 2AFH)	22.58	32.58	32.49
MgADP-bound FeP-MoFeP complex - molecule 1 in the asymmetric unit (3.1 Å / 2AFI)	32.42	45.70	45.67
MgADP-bound FeP-MoFeP complex - molecule 2 in the asymmetric unit (3.1 Å / 2AFI)	33.44	46.89	46.53
MgAMPPCP/MgADP-bound FeP-MoFeP complex (1.9 Å / 4WZA)	23.93	37.40	31.48
MgAMPPCP-bound FeP-MoFeP complex (2.3 Å / 4WZB)	27.35	45.01	37.91
Crosslinked FeP-MoFeP complex (3.2 Å / 1M1Y)	52.60	57.09	68.55
MgADP.AlFx -stabilized MoFeP-FeP complex – molecule 1 in the asymmetric unit (2.30 Å / 1M34)	33.45	44.61	48.94
MgADP.AlFx -stabilized MoFeP-FeP complex – molecule 2 in the asymmetric unit (2.30 Å / 1M34)	33.55	44.62	49.50